Eight-Element Dual-Polarized MIMO Slot Antenna System for 5G Smartphone Applications

Naser Ojaroudi Parchin[1], Yasir I. A. Al-Yasir[1], Ammar H. Ali[1], Issa Elfergani[2], James M. Noras[1], Jonathan Rodriguez[2,3] Senior, IEEE, and Raed A. Abd-Alhameed[1], Senior, IEEE

[1]Faculty of Engineering and Informatics, University of Bradford, Bradford, UK
[2]Instituto de Telecomunicações, Aveiro, Portugal
[3]University of South Wales, Pontypridd, CF37 1DL UK

Corresponding author: Naser Ojaroudi Parchin (e-mail: N.OjaroudiParchin@Bradford.ac.uk).

ABSTRACT In this manuscript, we propose an eight-port/four-resonator slot antenna array with dual-polarized function for multiple-input multiple output (MIMO) 5G mobile terminals. The design is composed of four dual-polarized square-ring slot radiators fed by pairs of microstrip-line structures. The radiation elements are designed to operate at 3.6 GHz and are located on the corners of the smartphone PCB. The square-ring slot radiators provide good dual-polarization characteristic with similar performances in terms of fundamental radiation characteristics. In order to improve the isolation and also reduce the mutual coupling characteristic between the adjunct microstrip-line feeding ports of the dual-polarized radiators, a pair of circular-ring/open-ended parasitic structures is embedded across each square-ring slot radiator. The -10 dB impedance bandwidth of each antenna-element is 3.4-3.8 GHz. However, for -6 dB impedance bandwidth, this value is 600 MHz (3.3-3.9 GHz). The proposed MIMO antenna offers good S-parameters, high-gain radiation patterns and sufficient total efficiencies even though it is arranged on a high-loss FR-4 dielectric. The SAR function and radiation characteristics of the proposed design in the vicinity of user-hand/user-head are studied. A prototype of the proposed smartphone antenna is fabricated and good measurements are provided. The antenna provides good features with a potential application for use in the 5G mobile terminals.

INDEX TERMS 5G, dual-polarized antenna, MIMO system, mobile terminal, ring slot antenna.

I. INTRODUCTION

MIMO wireless technology can highly improve the data rate, capacity, and link reliability of wireless systems through multi-path data transmission and reception. MIMO system is currently employed in 4G user equipment and is a promising technology for use in the future 5G mobile terminals [1-2]. One of the promising frequency bands for sub-6-GHz MIMO 5G communications is 3.4-3.8 GHz which has been proposed by Ofcom, UK [3].

There are many requirements of antenna designing such as low-profile, ease of fabrication, and high-isolation which must be considered to design a qualified MIMO antenna system for smartphones [4]. Recently, several works were reported in the literature for 5G mobile terminals [5-10]. However, all these antennas either provide narrow impedance bandwidth or use multiple radiators with single-polarization at different sides of PCB which occupy a huge space or increase the complexity of the MIMO system. A

multiple-antenna design for 5G smartphones applications is proposed in [11] which is only covering 3.5 to 3.7 of 5G bands and also the maximum mutual coupling of the antenna elements is -10 dB which could affect wireless system performance, antenna efficiency, as well as amplitude and phase of the radiators. Gap-coupled loop antenna array design with an impedance bandwidth of 3.4-3.8 GHz has been proposed in [12] for the future smartphone application. However, since the design is not planar, fabrication of this kind of antennas would be a challenging issue for the antenna engineers. In [13], an eight-port MIMO antenna with dual-polarized function has been proposed for 5G smartphone Applications. Its bandwidth is very narrow and not wide enough to cover more than 100 MHz. In addition, the radiators of the antenna cannot cover both sides of the mobile-phone PCB, since they are patch antennas. Another design of dual-polarized MIMO antenna with narrow

bandwidth and non-planar structure is proposed in [14]. Furthermore, the reduction of the mutual coupling between the closely-spaced radiators is not investigated in most of the recently published papers about 5G mobile terminals. Wide bandwidth, low mutual coupling, and compact size are some of the major characteristics concerned for designing a dual-polarized antenna [15]. We propose here a new design of a compact MIMO slot antenna system using four-radiator/eight-port dual-polarized antennas which provide wide bandwidth and improved isolation properties.

Slot antennas have become very attractive candidates for wireless systems owns lots of interesting features like simple structure, wide impedance bandwidth, good isolation, easy integration with active devices, and etc. Due to the fact that cutting a slot in the bottom layer of an antenna lets it radiates on both sides of the substrate, makes the slot antenna a good choice for designing the dual-polarized antenna to be used in wireless communication platforms [16]. Moreover, compared with the other conventional antennas (such as Dipole, Monopole, Yagi, and etc.) it is much easier to achieve the dual-polarized characteristic for the slot antenna with the microstrip-line feeding [17].

The configuration of the dual-polarized slot antenna element contains a compact square-ring slot antenna fed by rectangular microstrip-lines. In addition, a pair of circular-ring/open-ended parasitic structures has been employed across the ring slot to reduce the mutual coupling characteristic between two microstrip-line feeding ports. For the proposed 5G antenna, the ring-slot radiators are placed at four corners of the PCB to provide full radiation coverage with different polarizations. The single-element and the proposed antenna array exhibit good characteristics for MIMO applications. Their fundamental properties have been investigated in the following Sections. In addition, the radiation characteristics of the smartphone antenna array system in the presence of human hands/head have been studied and good results are achieved. Furthermore, the proposed MIMO antenna exhibits good SAR characteristic with low levels over the entire operation band that makes it suitable for use in the cellular applications.

II. DUAL-POLARIZED SINGLE-ELEMENT ANTENNA

In this section, the fundamental properties of the single element dual-polarized square-ring slot resonator with various design parameters have been studied and the simulation and measurement results are presented. Figure 1 illustrates a transparent view of the antenna configuration. As seen, the antenna configuration is composed of a square-ring slot in the ground plan with a pair of rectangular microstrip-lines employed at different top-side of the slot resonator. Furthermore, a pair of parasitic structures is used across the square-ring slot resonator on the top layer of the antenna. The antenna has a low profile of $W_S \times W_S$ and has been designed on an FR4 dielectric with relative permittivity 4.4, loss tangent 0.025 and thickness 1.6 mm. The parameter values of the single-element antenna and also the proposed MIMO array are specified in Table I.
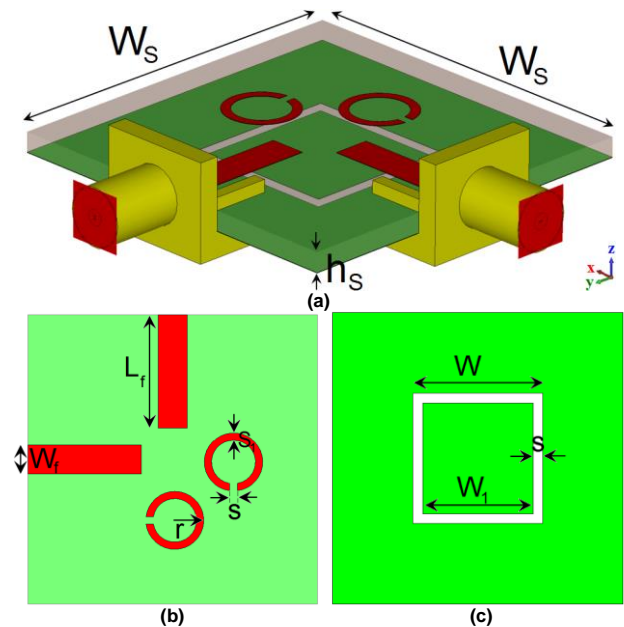

FIGURE 1. The proposed slot antenna configuration, (a) side-view, (b) top-layer, and (c) bottom-layer.

TABLE I
THE VALUES OF THE DESIGN PARAMETER

Parameter	Value (mm)
W	13.4
h_S	1.6
W_f	3
L_f	11.75
W_S	30
W_1	11.9
W_2	13.15
S	0.75
S_1	0.75
L_1	9
d	5.95
r	3

Each port of the proposed slot antenna provides a linear-polarization. The polarization type (vertical or horizontal) of each port relates to the placement of the antenna in the RF system. The configurations of the various structures studied for designing the dual-polarized microstrip-fed slot antenna were displayed in Fig. 2. The simulated S-parameters for a conventional dual-polarized microstrip-fed square-ring slot antenna (Fig. 2(a)), the antenna with only one circular-ring/open-ended parasitic structure (Fig. 2(b)), and the proposed single-element dual-polarized slot antenna structure (Fig. 2(c)) are illustrated and compared in Fig. 3. As illustrated, by employing the proposed parasitic structures on the top layer of the FR-4 dielectric and across the slot radiator, the desired impedance bandwidth, covering the frequency range of 3.4-3.8 GHz is obtained for the antenna with different ports and polarizations. In addition, as can be found, the mutual coupling characteristic between the feeding ports of the dual-polarized square-ring slot antenna has been reduced significantly (from -13 dB to -23 dB).
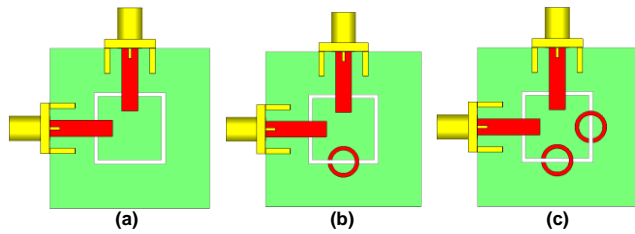
FIGURE 2. Ordinary square-ring dual-polarized antenna, (b) the antenna with a parasitic structure, and (c) the proposed design.
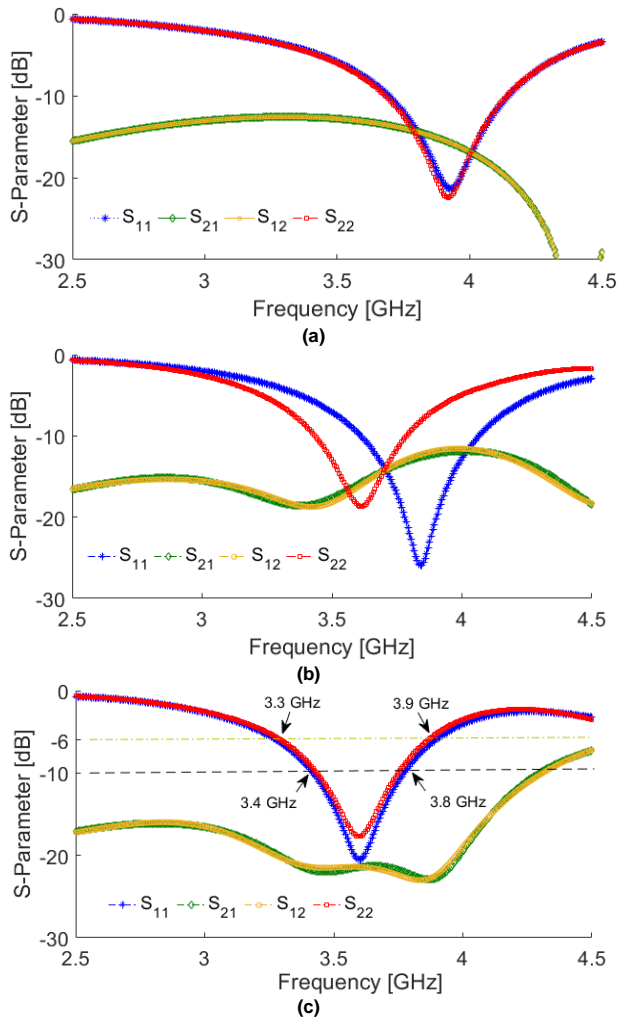

FIGURE 3. S-parameter results for the various designs illustrated in Fig. 2, respectively.
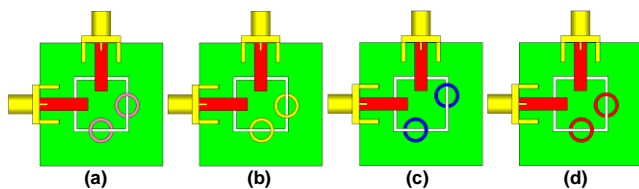

FIGURE 4. Different placement of the circular-ring/open-ended parasitic structures across the slot resonator.

The antenna performance for different positions of the embedded parasitic structures across the square-ring

resonator (Fig. 4) has been studied in Fig. 5. As illustrated, the antenna frequency response and also the mutual coupling characteristics are highly depended on the location of the parasitic structures. Furthermore, as seen, the fourth configuration (Fig. 4 (d)) is the best choice and representing the highest coupling with similar S_{11}/S_{22} characteristics for the desired frequency range (3.4-3.8 GHz 5G band).
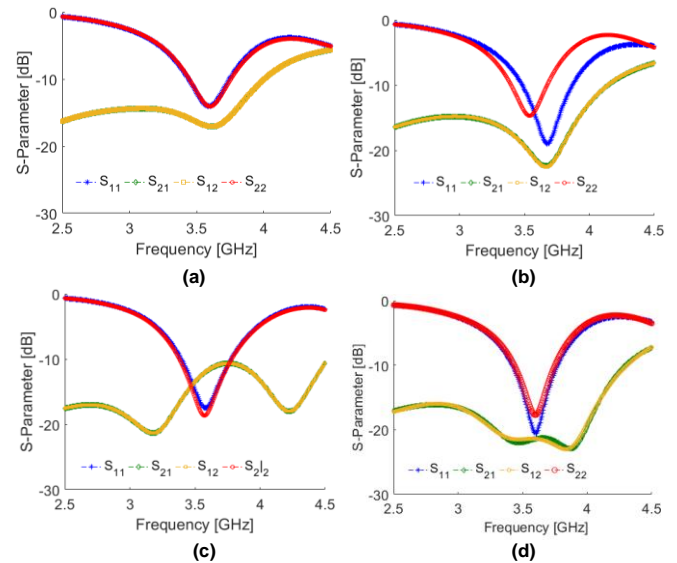

FIGURE 5. S-parameter results of the antenna for different positions of the parasitic structures shown in Fig. 4.

There are various design parameters of the proposed square-ring microstrip-fed slot antenna which have significant impacts on the antenna characteristics in terms of the operating band, the mutual coupling, and the impedance matching. The S_{11} characteristics of the antenna for various values of fundamental design parameters are studied in Fig. 6 and the obtained results have been discussed in the following.

One fundamental parameter relates to the length of the feed-lines (L_f). As seen in Fig. 6 (a), the feed-line length (L_f) impacts the impedance matching characteristic and for the values from 8.75 to 10.25 mm, the impedance matching function of the antenna reflection coefficient (S_{11}) can be tuned from less than -5 dB to more than -40 dB. The simulated S_{11} curves for different sizes of the slot-ring (W) are shown in Figure 6 (b): when its size decreases from 12.4 mm to 10.4 mm, the center of the operation frequency varies from 4.8 to 3.2 GHz while maintaining good impedance matching characteristic.

Another important parameter which tunes the operation frequency is the width of the ring slot (S_1). As illustrated in Fig. 6 (c), the antenna response can be also easily tuned by changing the width of the square-ring slot. As mentioned above, the circular-ring/open-ended parasitic structures are embedded on the top layer and across the square-ring slot radiators and as shown in Fig. 6 (d), their radius (r) can affect not only the operation frequency but also the bandwidth of the proposed design.
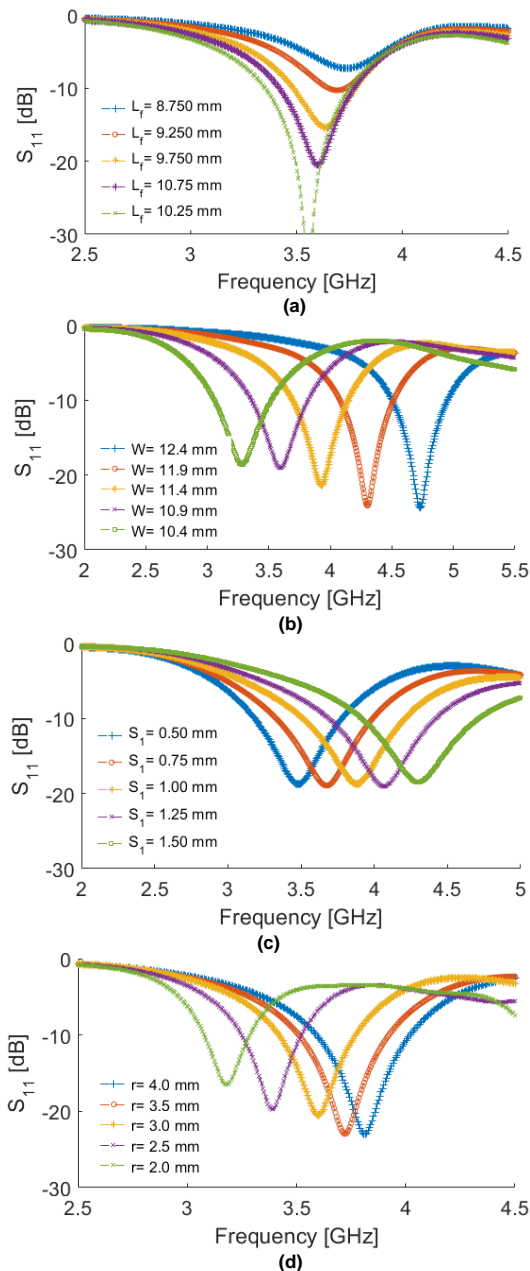
FIGURE 6. Antenna S_{11} results for different values of (a) L_f, (b) W, (c) S_1, and (d) r.

Figure 7 illustrates the current distributions of the dual-polarized ring slot antenna at the resonance frequency (3.6 GHz) in the top and bottom layers. As depicted in Figs. 7(a) and 7(b), most of the currents have been distributed around the square-ring slot radiator in the ground plane. It can be seen for the different feeding ports, the currents flow contrary to each other and provide the dual polarization characteristic [18]. In addition, as shown, the employed parasitic structures have high current densities and appear very active at 3.6 GHz.

The 3D views of the antenna radiation patterns at 3.6 GHz for different ports are displayed in Fig. 8. As shown, same radiation performances with different polarizations and also 3.97 dBi directivity are obtained for the proposed slot antenna

design. It can be seen that the designed slot antenna provides dumbbell-shaped radiation patterns suitable to cover the top and bottom side of the smartphone PCB which can increase the radiation coverage of the 5G MIMO antenna design. The maximum gain and efficiencies for the differently-fed square-ring slot antenna are represented in Fig. 9. As seen, the antenna provides high efficiencies even though it is designed on the FR-4 dielectric. In addition, as can be observed, the antenna exhibits around 3 dBi maximum gain.
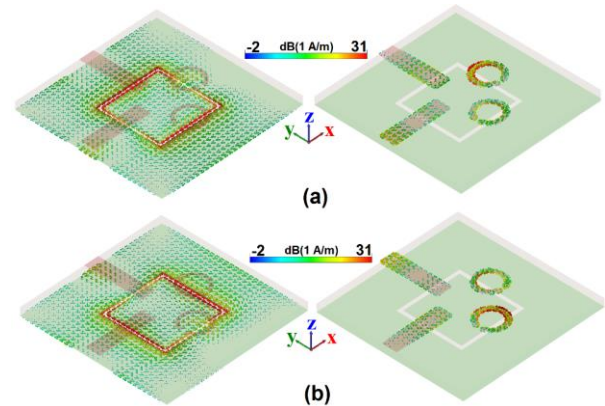

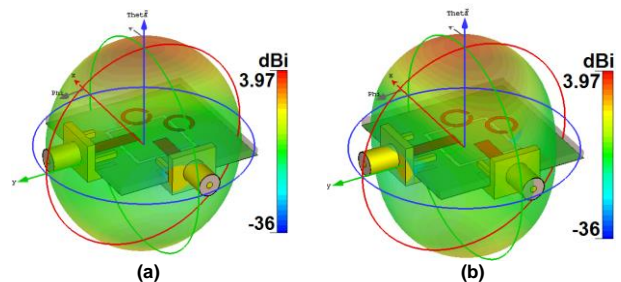**FIGURE 7.** Current distribution at 3.6 GHz for (a) port 1 and (b) port 2.

FIGURE 8. 3D transparent schematic of the antenna radiation patterns at 3.6 GHz for (a) port 1 and (b) port 2.
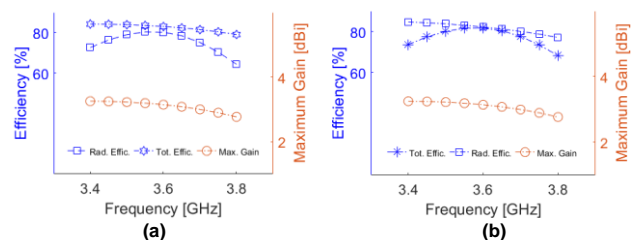

FIGURE 9. Efficiencies and maximum gains for (a) port 1 and (b) port 2.

As illustrated in Fig. 10, a prototype of the single-element dual-polarized slot antenna was fabricated and its fundamental characteristics were tested in the Antenna Laboratory at the University of Bradford. Figures 11 (a) and (b) show the measurement setups used for the antenna S-parameter and radiation characteristics, respectively. As can be seen, the S-parameters of the antenna including S_{11}/S_{22} and S_{21}/S_{12} characteristics were measured using the network analyzer and the antenna radiation pattern was measured in the anechoic chamber.
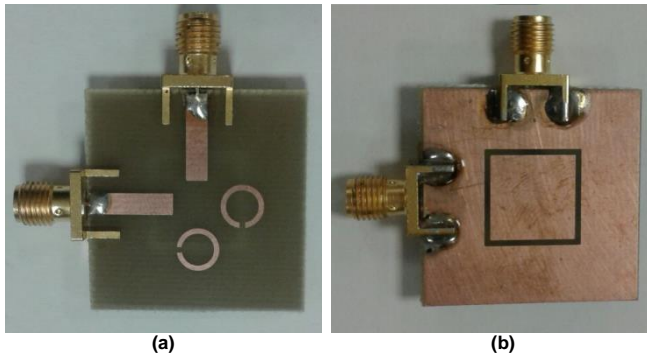
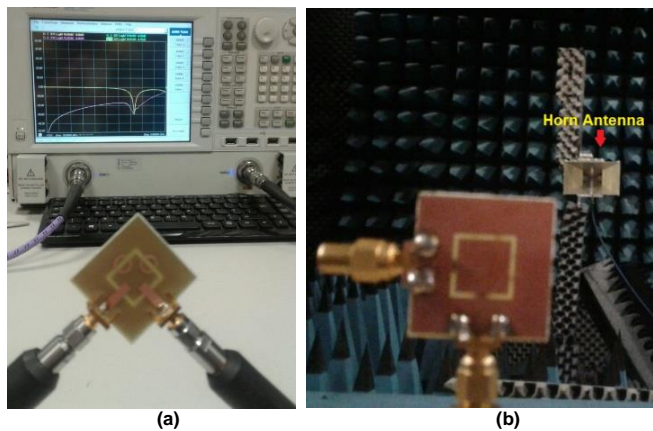**FIGURE 10.** Fabricated antenna, (a) top view and (b) bottom view.

FIGURE 11. Measurement setups for (a) S-parameter and (b) radiation pattern of the fabricated antenna element.
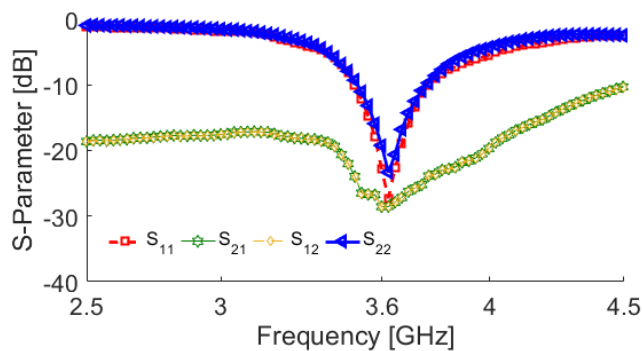

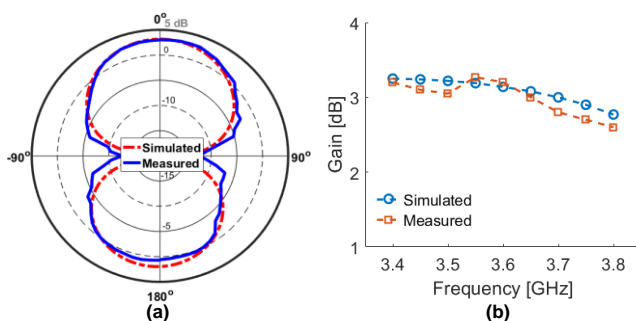**FIGURE 12.** Measured S-parameters of the antenna element.

FIGURE 13. Measured and simulated (a) antenna radiation patterns and (b) its gain levels.

The measured S-parameter results of the prototype are displayed in Fig. 12. As illustrated, the antenna provides very good impedance matching around 3.6 GHz (center frequency of the desired frequency band). High-isolation with more than -25 dB mutual coupling has been obtained for the fabricated sample. In addition, compared with the simulations (shown in Fig. 3 (c)), it can be confirmed that there is a good agreement between them. Figure 13 (a) shows the measured and simulated radiation patterns of the fabricated prototype at 3.6 GHz. As shown, the antenna exhibits a dumbbell-shaped radiation pattern with almost symmetrical schematic covering the top/bottom portions of the substrate. More than 3 dB IEEE gain with acceptable agreement has been achieved for the simulated and measured antenna radiation patterns. The simulation and measurement results of the antenna gain versus operation frequency are plotted in Fig. 13 (b). As shown, the antenna gain is almost constant and slightly varies around 3 dB.

III. THE PROPOSED MIMO 5G SMARTPHONE ANTENNA

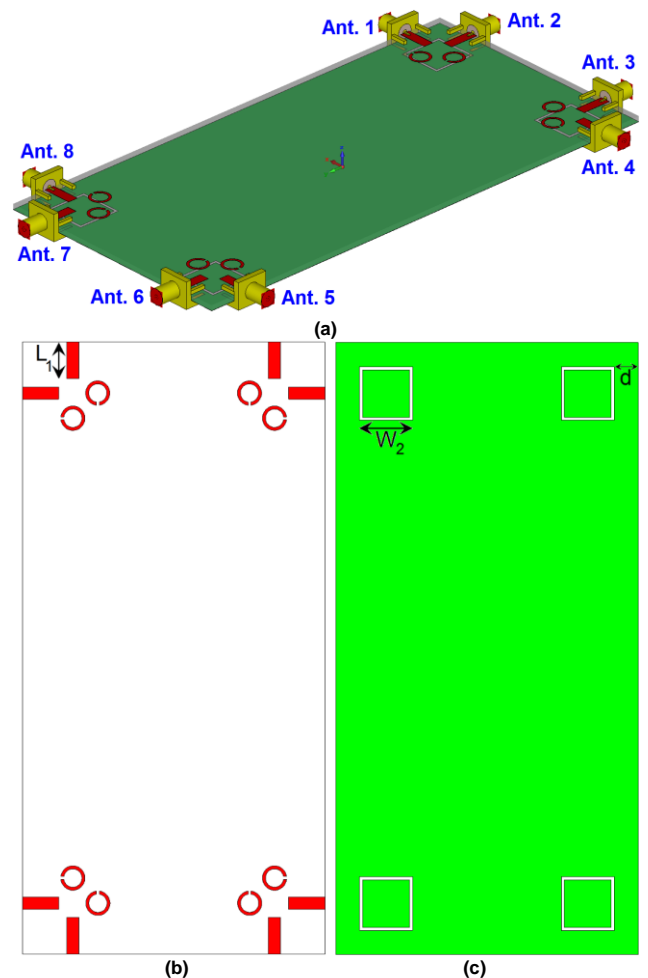Figure 14 displays the schematic of the proposed dual-polarized smartphone 5G antenna.

FIGURE 14. (a) 3D side view, (b) top and (b) bottom layers of the proposed 5G smartphone antenna.

The proposed design is arranged on an FR4 dielectric with permittivity 4.4 and loss tangent 0.025 which has an overall dimension of 75×150 mm^2. The dual-polarized square-ring slot antenna elements with the reduced size of 25×25 mm^2 are placed at the corners of the smartphone PCB.

The simulated S-parameters including the reflection coefficient (S_{nn}) and the mutual coupling (S_{nm}) characteristics of the designed dual-polarized MIMO antenna array are shown in Fig. 15. Clearly, the radiation elements have similar return loss performances providing high impedance matching (around -20 dB reflection coefficients) at 3.6 GHz. Furthermore, as shown in Fig. 15 (b), the mutual coupling function of the antenna elements (less than -15 dB) are good enough to avoid the loss of radiation performance for the 5G smartphone antenna.
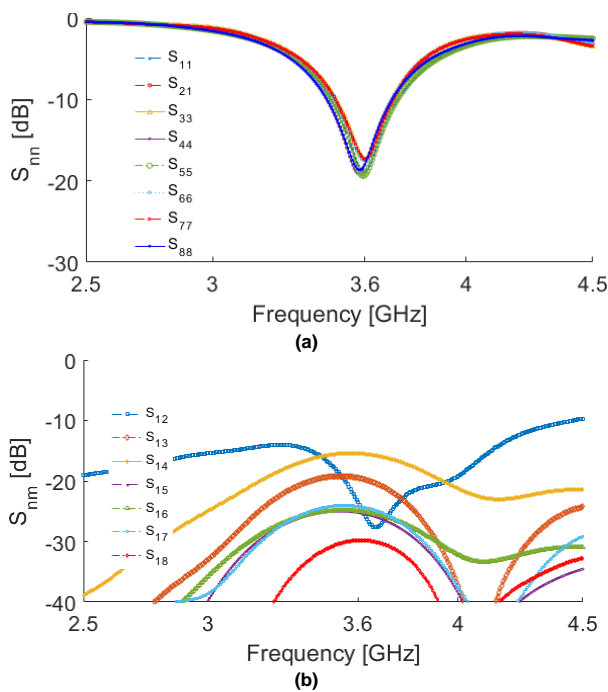

(a)

(b)

FIGURE 15. The antenna S-parameter results, (a) S_{nn} and (b) S_{nm}.
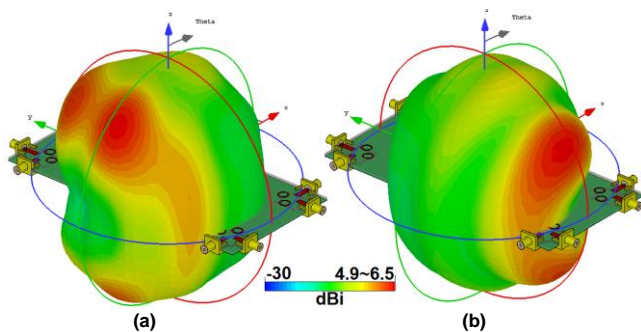

(a) **(b)**

FIGURE 16. 3D radiation patterns (with directivity values) of a slot radiator with different feeding ports (a) port 1 and port (2).

Employing the slot radiators on the proposed 5G array configuration not only exhibits sufficient bandwidth but also provides almost symmetrical radiation patterns to cover the top and bottom regions of the PCB. As shown in Fig. 16, the

antenna elements can provide high directivity radiation patterns covering the top and bottom sides of PCB and improving the coverage efficiency function [19].

Figure 17 displays the 3D top-views of the radiation patterns for each antenna elements deployed in the proposed 5G smartphone PCB. It can be seen, each side of the smartphone PCB can be covered by the radiation patterns of the radiators. At the same time, due to the dual-polarized characteristic of the antenna elements, different polarizations for each region of the PCB can be achieved which make the MIMO antenna system suitable for the future mobile terminal applications.
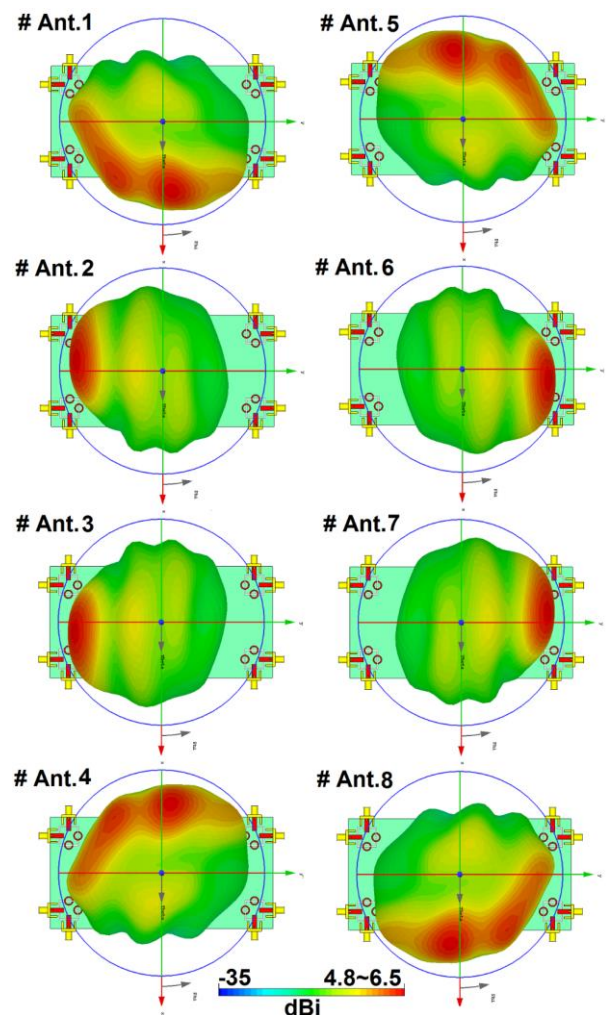

FIGURE 17. Radiation patterns for the antenna elements with directivity values at 3.6 GHz.

The radiation and total efficiencies of the dual-polarized antenna elements are illustrated in Fig. 18. As illustrated, the antenna elements have high radiation efficiencies. They also provide more than 70% total efficiencies at the resonance frequency (3.6 GHz). Furthermore, for the frequency range from 3.4 to 3.8 GHz (5G operation band), more than 75% radiation efficiency and 60% total efficiency characteristics have been achieved for the radiators of the proposed MIMO smartphone antenna.
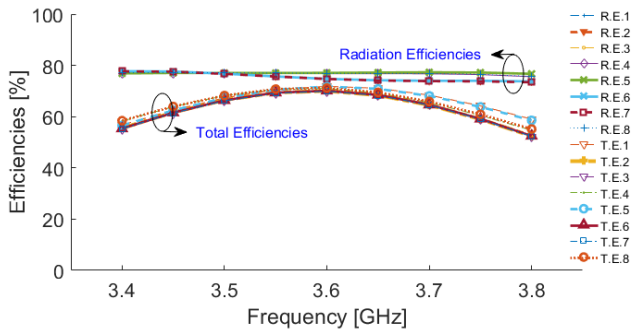
FIGURE 18. Efficiencies of the antenna elements.

The proposed smartphone 5G antenna design was properly fabricated on an FR-4 substrate and its properties in terms of radiation patterns and S-parameters were measured. Figures 19 (a) and 19 (b) illustrate the top and bottom views of the fabricated MIMO antenna system. In order to measure the system characteristics and also to avoid the mutual effect from the adjacent elements, 50-Ohm RF loads have been used for the antenna elements which are not under test. Figure 19 (c) shows the schematic of the MIMO system platform for measurement.
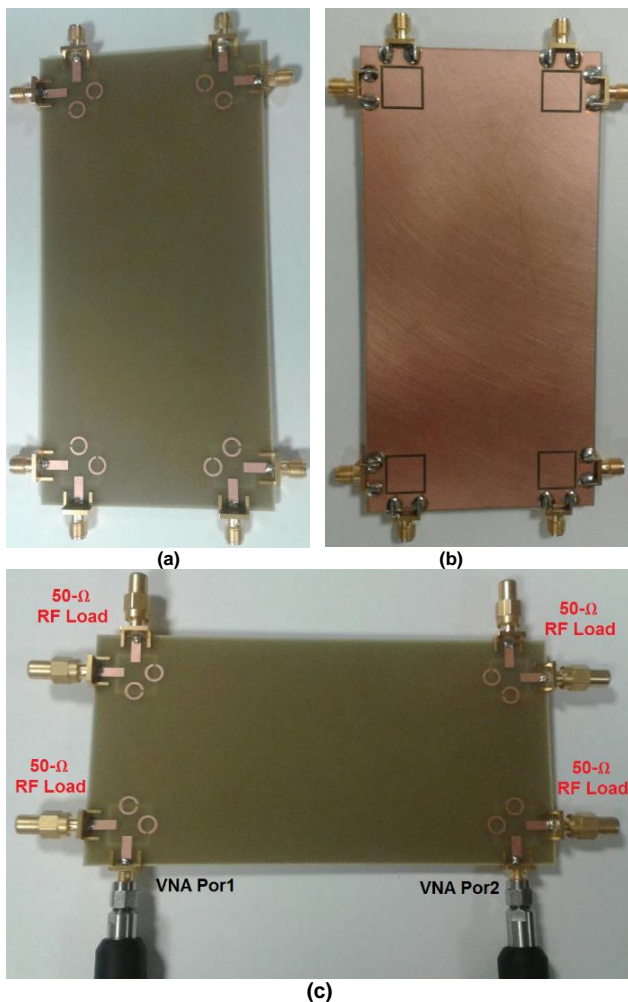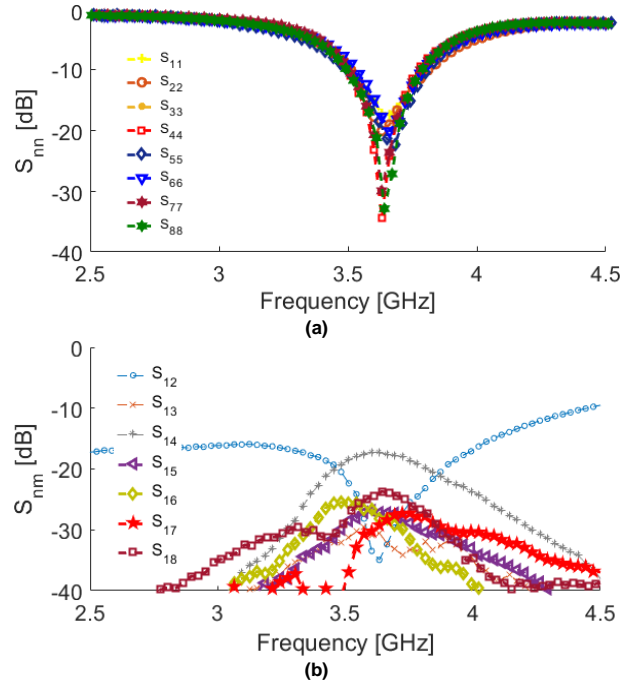

(a)

(b)

FIGURE 20. Measured S-parameter results of the proposed smartphone MIMO antenna, (a) S_{nn} and (b) S_{nm}.

As shown, a pair of the antennas has been connected to the Network Analyzer cables to be tested. The measured S-parameters (S_{nn}/S_{nm}) of the MIMO antenna system are illustrated in Fig. 20. As can be observed, each single element of the MIMO design has sufficient S-parameter characteristics and in compared with the simulated results, the agreement is acceptable.
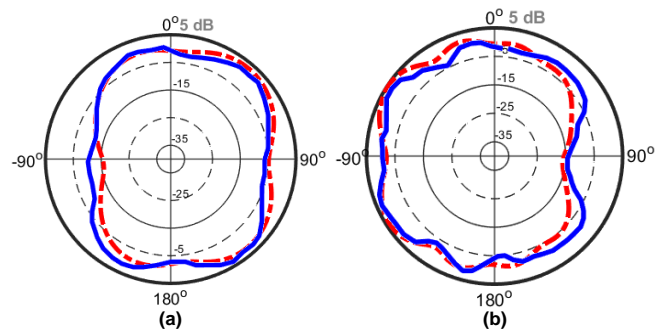

(a)

(b)

FIGURE 21. Measured (solid-lines) and simulated (dashed-line) 2D-polar radiation patterns of (a) antenna 1 and (b) antenna 2.

As can be seen from the 3D radiation patterns in Fig. 18, the slot antenna elements with the same polarizations provide almost the same performances. Due to this point, 2D polar radiation patterns of the adjacent microstrip-fed slot antennas with different polarizations have been measured. Figure 21 illustrates the simulation and measurement results of the antenna radiation patterns at 3.6 GHz. As can be seen, the fabricated prototype provides good radiation patterns similar to the simulated results. Furthermore, as seen, around 5 dB gain is obtained for the square-ring slot element with different polarizations.

(a) **(b)**

(c)

FIGURE 19. Fabricated smartphone antenna PCB, (a) top view, (b) bottom view, and (c) the prototype connected to the cables and loads.

The envelope correlation coefficient (ECC) of diverse antenna pairs is a typical function to judge multiple port performance of the MIMO antenna. The correlation among the embranchment signals received by different antennas is evaluated by this parameter, and lower ECC means more diversified patterns as a rule [20]. An acceptable standard for a desirable MIMO system is ECC < 0.5. Total active reflection coefficient (TARC) is another important parameter which must be also considered in MIMO antennas. The calculated ECC and TARC results of the proposed MIMO design form the simulations and measurements are presented in Fig. 22. The obtained results indicate that the calculated ECC function of the MIMO antenna elements is very low over the entire operating band. In addition, the results from the calculated TARC show that the higher mutual coupling can result in the higher TARC.
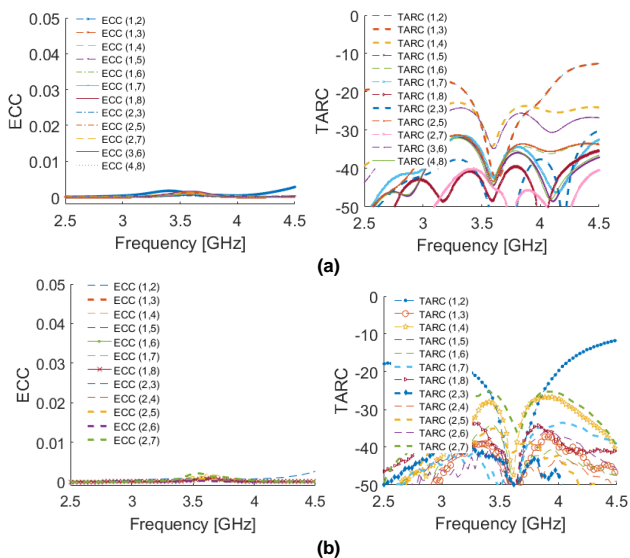

FIGURE 22. (a) Simulated and (b) Measured ECC and TARC results.

IV. USER-IMPACT AND SAR INVESTIGATION

Due to the importance of the user-impact on the radiation properties of a smartphone antenna system and also the specific absorption rate (SAR) effects of the smartphone antenna on the human head [21], the investigation on these parameters have been studied in this section. Figure 23 investigates the performance of the proposed MIMO smartphone antenna in terms of the total efficiency characteristic under right-hand mode (RHM) and left-hand mode (LHM) scenarios.

According to the simulations, the antenna elements show good performances in the vicinity of the user-hand and provide sufficient total efficiencies. The maximum reductions in total efficiently characteristic have been occurred for the antenna elements partially covered by hand tissue, especially Antennas 5 and 6 in RHM and Antennas 7 and 8 in LHM. It should be emphasized that this behavior is mainly because of hand tissue properties that is very lossy and can absorb the radiated power of the antenna. However, they still provide at least 20% total efficiency in 3.6 GHz and

can still work in MIMO cellular communications. In addition, compared with the simulated total efficiencies, the performances of the antennas close to the finger have been reduced more than the elements far from the user's hand and fingers.
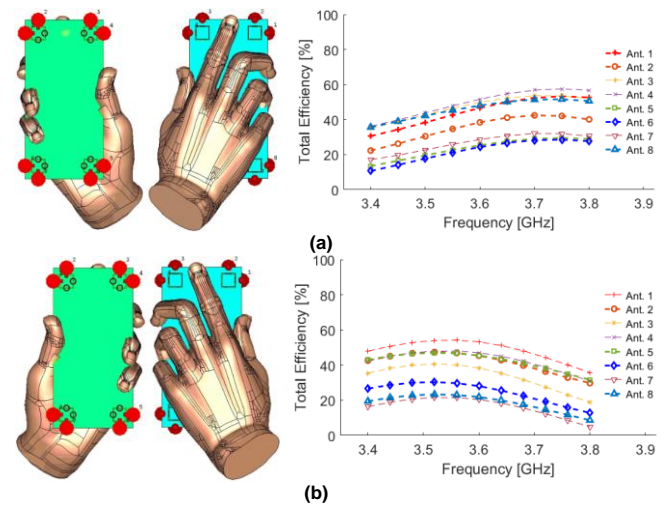

FIGURE 23. (a) Right Hand and (b) Left hand modes with the simulated efficiency results.

Figure 24 illustrates the radiation patterns of the antenna elements in the vicinity of the user's double-hands (read mode). As illustrated, the antenna elements provide good radiation patterns with sufficient gain values and pattern coverage. Clearly, the user's hand reduced the characteristics of the antenna, however, it is not very significant in this study. As seen, the antenna elements exhibit variable gain values with more than 1.9 dB.
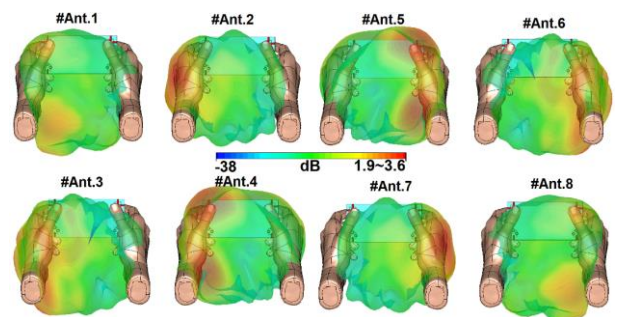

FIGURE 24. Radiation patterns of the different elements in Read-Mode.

SAR is the measurement function for the electromagnetic absorption of a human body during transmit and receive radio frequency data which is a critical issue for mobile terminal systems and should be as low as possible [22]. The simulated SAR values for the proposed design in the vicinity of the human-head at different frequencies are investigated in Fig. 25. As can be observed, the antenna has sufficient SAR values for the frequencies of 3.4, 3.6, and 3.8 GHz. The distance between MIMO antenna and the human-head in the z-axis has a significant impact on the SAR values. It should be noted that the distance in this study is less than 10 mm.

Figure 26 depicts the radiation patterns for each antenna element of the proposed MIMO system in Talk-Mode (in the presence of user-hand/user-head). As seen, the proposed MIMO antenna system works well and provides sufficient gain values for each radiator used at different corners of the PCB. The obtained IEEE gain for the antenna elements varies from 1.3 to 4 dB and mainly depends on the locations of the antenna elements in the Talk-Mode scenario.
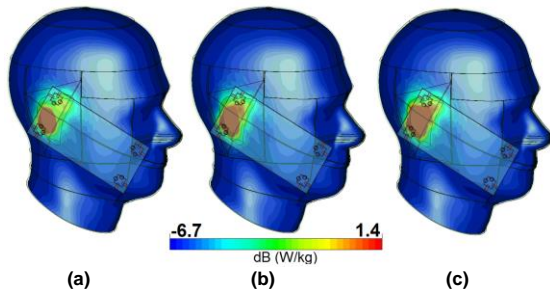

FIGURE 25. SAR investigation of the proposed MIMO antenna at, (a) 3.4 GHz, (b) 3.6 GHz, and (c) 3.8 GHz.
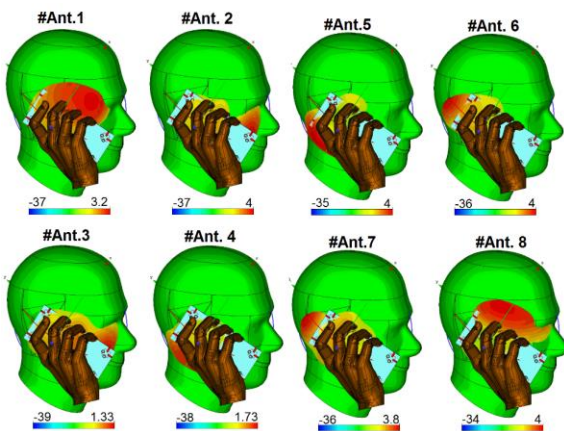

FIGURE 26. The radiation pattern of the antenna elements in Talk-Mode.

V. CONCLUSION

In this manuscript, a new design of reduced-coupling slot antenna array has been proposed for 5G MIMO mobile terminals. The structure of the proposed MIMO antenna was composed of dual-polarized square-ring slot antennas placed at the corners of the smartphone PCB. In order to reduce the mutual coupling of the antenna elements, a pair of circular-ring/open-ended parasitic structures was used on the top layer of the dielectric and across the square-ring slot radiator. Using the embedded parasitic structure, the mutual coupling of the adjacent radiators has been reduced significantly. The proposed MIMO antenna provides sufficient radiation coverage with dual-polarization at each side of the PCB. The MIMO antenna system was fabricated and tested and good agreements have been achieved between the simulation and measurements. Good radiation performances have been obtained for the MIMO antenna in the presence of user-head/user-hand. The proposed antenna offers sufficient characteristics for 3.6 GHz applications and might be a suitable candidate for use in 5G smartphone applications.

REFERENCES

[1] Q. U. A. Nadeem et al., "Design of 5G full dimension massive MIMO systems," *IEEE Trans. Commun.*, vol. 66, no. 2, pp. 726–740, Feb. 2018.

[2] A.Osseiran, *et al.*, "Scenarios for 5G mobile and wireless communications: the vision of the METIS project," *IEEE Commun. Mag.,* vol. 52, pp. 26-35, 2014.

[3] "Ofcom," 8 February 2017. [Online]. Available: https://www.ofcom.org.uk/.

[4] H. H. Yang and Y. Q. S. Quel, "Massive MIMO Meet Small Cell," *SpringerBriefs in Electrical and Computer Engineering*, 2017. DOI 10.1007/978-3-319-43715-6_2

[5] Z. Qin, W. Geyi, M. Zhang, and J. Wang, "Printed eight-element MIMO system for compact and thin 5G mobile handest," *Electron. Lett.*, vol. 52, no. 6, pp. 416-418, Mar. 2016.

[6] Y. Li, H. Zou, M. Wang, M. Peng, G. Yang, "Eight-element MIMO antenna array for 5G/Sub-6GHz indoor micro wireless access points," *2018 International Workshop on Antenna Technology (iWAT)*, 5-7 March 2018, Nanjing, China.

[7] R. Hussain, A. T. Alreshaid, S. K. Podilchak, and M. S. Sharawi, "Compact 4G MIMO antenna integrated with a 5G array for current and future mobile handsets," *IET Microw. Antennas Propag.*, vol. 11, no. 2, pp. 271-279, 2017.

[8] A. A. Al-Hadi, J. Ilvonen, R. Valkonen, V. Viikan, "eight-element antenna array for diversity and MIMO mobile terminal in LTE 3500MHz band," *Microwave Opt. Technol. Lett.*, vol. 56, pp. 1323-1327, 2014.

[9] K.-L. Wong, J.-Y. Lu, L.-Y. Chen, W.-Y. Li, Y.-L. Ban, and C. Li, "16-antenna array in the smartphone for the 3.5-GHz MIMO operation," *in Proc. Asia–Pacific Microw. Conf.*, Nanjing, China, Dec. 2015, pp. 1–3.

[10] L. Sun, *et al.*, "Compact 5G MIMO Mobile Phone Antennas With Tightly-arranged Orthogonal Mode Pairs," *IEEE Trans. Antennas Propag.*, 2018, DOI 10.1109/TAP.2018.2864674.

[11] Y. Li, *et al.*, Multiband 10-Antenna Array for Sub-6 GHz MIMO Applications in 5-G Smartphones," *IEEE Access*, vol. 6, pp. 28041-28053, 2018

[12] K.-L. Wong, C.-Y. Tsai, and J.-Y. Lu, "Two asymmetrically mirrored gap-coupled loop antennas as a compact building block for eight-antenna MIMO array in the future smartphone," *IEEE Trans. Antennas Propag.*, vol. 65, no. 4, pp. 1765–1778, Apr. 2017.

[13] M,-Y. Li, "Eight-port orthogonally dual-polarised MIMO antennas using loop structures for 5G smartphone," *IET Microwaves, Antennas & Propagation*, vol. 11, pp. 1810-1816, 2017.

[14] M.-Y. Li *et al.*, "Eight-port orthogonally dual-polarized antenna array for 5G smartphone applications," *IEEE Trans. Antennas Propag.*, vol. 64, no. 9, pp. 3820-3830, Sep. 2016.

[15] Y. Liu, H. Yi, F. W. Wang, and S. X. Gong, "A novel miniaturized broadband dual-polarized dipole antenna for base station," *IEEE Antennas Wireless Propog. Lett.*, vol. 12, pp. 1335–1338, 2013.

[16] Y. Yoshimura, "A microstripline slot antenna," *IEEE Trans. Microwave Theory Tech.*, vol. MTT-20, no. 11, pp. 760 –762, Nov. 1972.

[17] D. M. Pozar, "A reciprocity method of analysis for printed slot and slot coupled microstrip antennas," *IEEE Trans. Antennas Propag.*, vol. AP-34, no. 12, pp. 1439 –1446, Dec. 1986.

[18] Z. N. Chen, and X. M. Qing, "Dual-band circularly polarized S-shape slotted patch antenna with a small frequency-ratio," *IEEE Trans. Antennas Propag.*, vol. 58, no. 6, pp. 2112–2115, Jun. 2010.

[19] X. Qing, Z. N. Chen, and T. S. P. See, "A multi-band MIMO antenna with full coverage," *EuCAP2011*, pp. 2497–2500, 2011.

[20] M. S. Sharawi, "Printed multi-band MIMO antenna systems and their performance metrics [wireless corner]," *IEEE Antennas Propag. Mag.*, vol. 55, no. 5, pp. 218–232, Oct. 2013.

[21] J. Moustafa, N. J. McEwan, R. A. Abd-Alhameed and P. S. Excell, "Low SAR phased antenna array for mobile handsets," *Applied Computational Electromagnetics Society (ACES) Journal*, vol. 21, pp. 196-205, 2006.

[22] M. Fallah, A. A. Heydari, A. R. Mallahzadeh, and F. H. Kashani, "Design and SAR reduction of the vest antenna using metamaterial for broadband applications," *Applied Computational Electromagnetics Society (ACES) Journal*, vol. 26, pp. 141-155, 2011.